

# Spectral density in a nematic state of iron pnictides

Maria Daghofer,<sup>1,\*</sup> Andrew Nicholson,<sup>2,3</sup> and Adriana Moreo<sup>2,3</sup>

<sup>1</sup>*IFW Dresden, P.O. Box 27 01 16, D-01171 Dresden, Germany*

<sup>2</sup>*Department of Physics and Astronomy, The University of Tennessee, Knoxville, TN 37996*

<sup>3</sup>*Materials Science and Technology Division, Oak Ridge National Laboratory, Oak Ridge, TN 32831*  
(Dated: May 4, 2012)

Using cluster-perturbation theory, we calculate the spectral density  $A(\mathbf{k}, \omega)$  for a nematic phase of models describing pnictide superconductors, where very short-range magnetic correlations choose the ordering vector  $(\pi, 0)$  over the equivalent  $(0, \pi)$  and thus, break the fourfold rotation symmetry of the underlying lattice without inducing long-range magnetic order. In excellent agreement with angle-resolved photo-emission spectroscopy (ARPES), we find that the  $yz$  bands at  $X$  move to higher energies. When onsite Coulomb repulsion brings the system close to a spin-density-wave (SDW) and renormalizes the band width by a factor of  $\approx 2$ , even small anisotropic couplings of 10 to 15 meV strongly distort the bands, splitting the formerly degenerate states at  $X$  and  $Y$  by  $\approx 70$  meV and shifting the  $yz$  states at  $X$  above the chemical potential. This similarity to the SDW bands is in excellent agreement with ARPES. An important difference to the SDW bands is that the  $yz$  bands still cross the Fermi level, again in agreement with experiment. We find that orbital weights near the Fermi surface provide a better characterization than overall orbital densities and orbital polarization.

PACS numbers: 74.70.Xa, 74.25.Jb, 71.27.+a, 71.10.Fd

## I. INTRODUCTION

In recent years, iron-based superconductors have been intensely studied,<sup>1,2</sup> because of their high superconducting transition temperatures. As in the cuprates, antiferromagnetic (AFM) order is present in the phase diagram and phonons are not believed to be strong enough to explain the high transition temperatures.<sup>3</sup> However, in the pnictides the AFM phase is a metallic spin-density wave (SDW) rather than a system of localized Heisenberg spins as is the case in the cuprates. At temperatures slightly above the transition to the SDW with ordering vector  $(\pi, 0)$  or  $(0, \pi)$ , many weakly doped compounds show an orthorhombic phase without long-range magnetic order, but with broken rotational symmetry. This phase has slightly different lattice constants along the in-plane iron-iron bonds,<sup>4</sup> but the anisotropy that develops in electronic observables such as resistivity<sup>5,6</sup> or angle-resolved photoemission spectroscopy (ARPES)<sup>7-10</sup> of detwinned samples appears considerably more pronounced.

A number of competing scenarios have been proposed for this phase and can be broadly categorized as “magnetism”, “orbital”, and “lattice” driven. In the first case, the symmetry between equivalent magnetic ordering vectors  $(\pi, 0)$  and  $(0, \pi)$  is broken and the system chooses one of them without immediately establishing long-range magnetic order.<sup>11,12</sup> In the second picture, it is the degeneracy between two  $d$  orbitals of the iron ion, the  $xz$  and  $yz$  states providing the greatest contribution to the states at the Fermi surface (FS), that is spontaneously broken;<sup>13</sup> the resulting orbital occupation then determines the effective magnetic exchange constants that generate the SDW order. Both pictures were first discussed in insulating spin and spin-orbital models and have since been generalized to take into account electron itineracy. Stud-

ies in several models have shown that nematic phases can indeed develop between structural and magnetic transition temperatures.<sup>14,15</sup>

While a definite answer about the driving mechanism may be hard to nail down, as spin, orbital,<sup>13,14</sup> and lattice<sup>15-17</sup> degrees of freedom are naturally coupled and interact with each other, one may nevertheless try to identify the dominant ingredient(s). To this end, it is instructive to establish how each type of symmetry breaking manifests itself in observables. If the symmetry breaking is assumed to mostly concern the  $xz$  and  $yz$  orbitals, one can introduce it explicitly by adding a phenomenological energy splitting between the orbitals and evaluating its impact on observables such as the optical conductivity or the spectral density. These signatures were found to qualitatively agree with experiments,<sup>18</sup> where states of  $yz$  character are found to be higher in energy than those of  $xz$  character in several different pnictide compounds from the two structurally slightly different “111” and “122” families. On the other hand, ARPES data taken above the Néel temperature have alternatively been interpreted in terms of “band folding” due to magnetic order<sup>9</sup> or emphasising the coupling between magnetic order and the orbital states near the Fermi level.<sup>10</sup> Short-range magnetic order<sup>19</sup> and the spin-nematic scenario<sup>20</sup> likewise reproduce the anisotropic conductivity, and the latter has been argued to lead to an effective orbital splitting.<sup>14</sup> However, a direct calculation of the spectral density in a nematic phase is so far lacking.

We use here a method that combines real and momentum space, cluster-perturbation theory (CPT),<sup>21,22</sup> to calculate the one-particle spectral density  $A(\mathbf{k}, \omega)$  for a spin-nematic phase where rotational symmetry is broken via (very) short-range spin correlations that are AFM in  $x$  and ferromagnetic (FM) in  $y$  direction

[corresponding to ordering vector  $(\pi, 0)$ ], but without long-range magnetic correlations beyond second neighbors. The obtained spectral density reproduces the momentum-dependence of the band shifting observed in ARPES.<sup>8–10</sup> If onsite interactions bring the system close to the SDW transition, a small phenomenological magnetic anisotropy leads to large anisotropies in  $A(\mathbf{k}, \omega)$ . Thus, we can theoretically describe the astonishing ARPES result that the overall band shifts characterizing  $A(\mathbf{k}, \omega)$  in the SDW phase are nearly fully developed already above the Néel temperature.<sup>8</sup>

In order to be able to solve the problem exactly on a small cluster, we use variants of models with three<sup>23</sup> and four<sup>24</sup> orbitals; models and method are introduced and discussed in Sec. II. Section III A discusses the anisotropic band shifts induced by (strong) anisotropic magnetic couplings in the non-interacting models; in Sec. III B, we show that in the presence of onsite interactions and near the SDW transition, smaller magnetic anisotropies have a large impact. In Sec. IV, our results are summarized and discussed.

## II. METHOD AND MODEL

The aim of the paper is to calculate the spectral density  $A(\mathbf{k}, \omega)$  in a phase where (short-range) magnetic correlations break the fourfold symmetry of the lattice, but without long-range magnetic order. The latter requirement prevents us from carrying out our calculations directly in momentum space, as it has been done for the paramagnetic and AFM phases. As an alternative approach, we choose here cluster perturbation theory.<sup>21,22</sup> In this method, the ground state and one-particle Green's function are evaluated (almost) exactly (with Lanczos exact diagonalization) for a fully interacting quantum model on a small cluster, and hoppings between clusters are treated in perturbation theory [for an illustration see Figs. 1(a) and 1(b)]. Apart from the limit of small inter-cluster hoppings, this approximation also becomes exact in the opposite limit of vanishing interactions, as can be seen by considering that it amounts to replacing the self energy of the full system by that of the small cluster.<sup>26</sup> Long-range order can be treated with the related variational cluster approach (VCA),<sup>26,27</sup> as it has been done for a two-orbital model for pnictides.<sup>28,29</sup>

The biggest drawback of the VCA is that correlations are only included exactly within the small cluster, while longer-range effects are treated at a mean-field level. For nematic phases with at most short-range order, this limitation turns into a huge *advantage*: We can break the symmetry between the  $x$  and  $y$  directions locally on the small cluster, see below, but without imposing long-range order by a symmetry-breaking field. If the small cluster is, e.g., an AFM coupled dimer, its groundstate is thus still given by a singlet, i.e., a superposition of “up-down” and “down-up”, which removes long-range correlations.

When using a dimer as the directly solved cluster, we

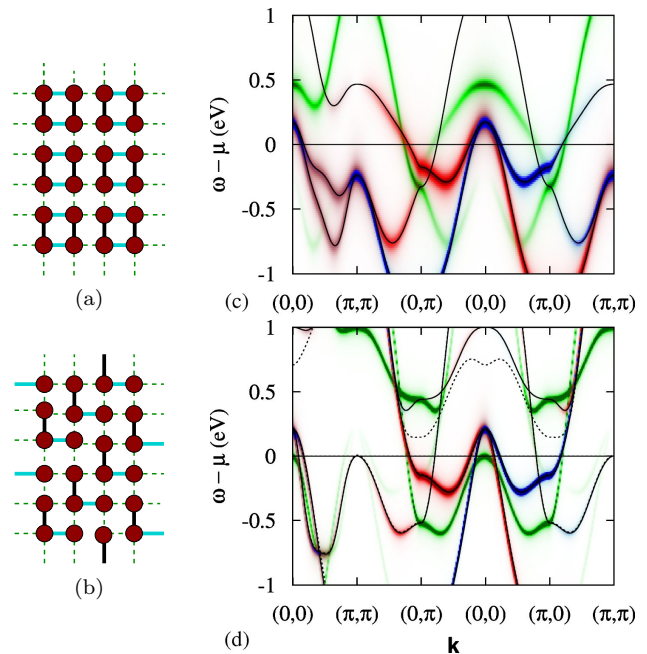


FIG. 1. (Color online) Schematic illustration of the cluster decomposition into (a) four-site and (b) three-site clusters used for the three- and four-orbital models. Ground-state energies and Green's functions of the small cluster – as connected by thick solid lines – are obtained by exact diagonalization. Clusters are then connected in CPT along the thinner dashed bonds. Within the cluster, AFM (FM) Heisenberg exchange acts between electrons along the  $x$ - ( $y$ -) bond. (c) Spectral density  $A(\mathbf{k}, \omega)$  of the non-interacting three-orbital model Eq. (4). Solid lines indicate the bands in terms of the pseudo-crystal momentum  $\tilde{\mathbf{k}}$ , shading the spectral weight in terms of “real” momentum  $\mathbf{k}$ , the difference is that weight with  $xy$  character shifts by  $(\pi, \pi)$ . [Note that along  $(0, 0)$ - $(\pi, \pi)$ , the bands with dominant  $xz/yz$  character contain these two orbitals with identical weight, even though the  $yz$  character – here drawn on top – dominates the figures.] (d)  $A(\mathbf{k}, \omega)$  of the non-interacting four-orbital model. Dashed lines indicate the results for the model that is obtained by removing<sup>24</sup> the  $3z^2 - r^2$  orbital from the five-orbital model of Ref. 25. Solid lines are for the model used here, where the  $x^2 - y^2$  orbital is then somewhat removed from the Fermi level by changing  $t_{xx}^{33}$  from  $-0.02$  to  $t_{xx}^{33} = 0.03$  and  $\epsilon_3$  from  $-0.22$  to  $-0.12$  (notation as in Ref. 25). As in (c), shading indicates the spectral weight for the “real” momentum instead of the pseudo-crystal momentum. In the online version, red refers to  $xz$ , blue to  $yx$ , and green to all other orbitals. In all spectra, peaks are broadened by a Lorentzian  $\delta/((\omega - \omega_0)^2 + \delta^2)$  with  $\delta = 0.05$  except for Fig. 1(d), where  $\delta = 0.025$ . All energies are in eV.

find instabilities, i.e., poles of the one-particle Green's function that are on the wrong side of the chemical potential. While this does not necessarily invalidate the results (which are in fact similar to the more stable results described below), it may indicate that the self energy of a dimer differs too strongly from that of a large two-dimensional system to provide a reliable approxima-

tion. In order to be able to use three- (four-) site clusters instead, which lead to stable results, we restrict the Hamiltonian to the four (three) orbitals that contribute most of the weight at the FS. The results presented here were obtained with the cluster decompositions shown in Figs. 1(a) and 1(b), but equivalent results were found for the three-orbital model when using a “brick-wall” arrangement of  $2 \times 2$  clusters instead of the “columns” in Fig. 1(a).

The momentum-dependent tight-binding Hamiltonian in orbital space can be written as

$$H_{\text{TB}}(\tilde{\mathbf{k}}) = \sum_{\tilde{\mathbf{k}}, \sigma, \mu, \nu} T^{\mu, \nu}(\tilde{\mathbf{k}}) d_{\tilde{\mathbf{k}}, \mu, \sigma}^\dagger d_{\tilde{\mathbf{k}}, \nu, \sigma}, \quad (1)$$

where  $d_{\tilde{\mathbf{k}}, \nu, \sigma}$  ( $d_{\tilde{\mathbf{k}}, \nu, \sigma}^\dagger$ ) annihilates (creates) an electron with pseudo-crystal momentum  $\tilde{\mathbf{k}}$  and spin  $\sigma$  in orbital  $\nu$ . The three-orbital model used here is based on the model of Ref. 23, but a few longer-range hoppings were added to provide a better fit of the bands near the FS, because the original three-orbital model has magnetic instabilities too far from  $(\pi, 0)/(0, \pi)$ .<sup>30</sup> The  $T^{\mu, \nu}(\tilde{\mathbf{k}})$  give the hoppings between orbitals  $\mu$  and  $\nu$  and are

$$T^{11/22} = 2t_{2/1} \cos k_x + 2t_{1/2} \cos k_y + 4t_3 \cos k_x \cos k_y \\ \pm 2t_{11}(\cos 2k_x - \cos 2k_y) + 4t_{12} \cos 2k_x \cos 2k_y, \quad (2)$$

$$T^{33} = \Delta_{xy} + 2t_5(\cos k_x + \cos k_y) + 4t_6 \cos k_x \cos k_y \\ + 2t_9(\cos 2k_x + \cos 2k_y) \\ + 4t_{10}(\cos 2k_x \cos k_y + \cos k_x \cos 2k_y), \quad (3)$$

$$T^{12} = T^{21} = 4t_4 \sin k_x \sin k_y, \quad (4)$$

$$T^{13} = \bar{T}^{31} = 2it_7 \sin k_x + 4it_8 \sin k_x \cos k_y, \quad (5)$$

$$T^{23} = \bar{T}^{32} = 2it_7 \sin k_y + 4it_8 \sin k_y \cos k_x, \quad (6)$$

where a bar denotes the complex conjugate. Hopping parameters are  $t_1 = -0.08$ ,  $t_2 = 0.1825$ ,  $t_3 = 0.08375$ ,  $t_4 = -0.03$ ,  $t_5 = 0.15$ ,  $t_6 = 0.15$ ,  $t_7 = -0.12$ ,  $t_8 = -t_7/2 = 0.06$ ,  $t_{10} = -0.024$ ,  $t_{11} = -0.01$ ,  $t_{12} = 0.0275$ ,  $\Delta_{xy} = 0.75$ ,  $\mu = 0.4745$ ; Fig. 1 shows the uncorrelated tight-binding bands. The four-orbital model was obtained by removing the  $3z^2 - r^2$  orbital<sup>24</sup> from the five-orbital model of Ref. 25 and slightly changing onsite energy and third-neighbor hopping of the  $x^2 - y^2$  orbital to alleviate the fact that removing the  $3z^2 - r^2$  orbital moves it too close to the Fermi level, see Fig. 1(d). In principle, hoppings can be extended to three dimensions and parameters could be fitted to model specific compounds, at least in the more detailed four-orbital model. The features we aim to study here – an anisotropy between the  $X$  and  $Y$  points – have been experimentally observed in different compounds, and we are going to see that both the three- and the four-orbital models lead to similar results despite their somewhat different dispersions, suggesting that fine-tuning of the kinetic energy is not crucial.

We use a unit cell with one iron atom to distinguish between momenta  $(\pi, 0)$  and  $(0, \pi)$ , which would both map

to  $(\pi, \pi)$  for a two-iron unit cell. Due to an internal symmetry of the two-iron unit cell,<sup>31,32</sup> it is always possible to use a one-iron unit cell for tight-binding models restricted to an Fe-As plane. However, the  $xz$  and  $yz$  orbitals with momentum  $\mathbf{k}$  couple to the other orbitals at momentum  $\mathbf{k} + (\pi, \pi)$ . Thus, one writes the tight-binding Hamiltonians in terms of a pseudo-crystal momentum  $\tilde{\mathbf{k}}$ , which is  $\tilde{\mathbf{k}} = \mathbf{k}$  for  $xz/yz$  and  $\tilde{\mathbf{k}} = \mathbf{k} + (\pi, \pi)$  for  $xy/x^2 - y^2/3z^2 - r^2$ . In real space, such a notation corresponds to a local gauge transformation, where replacing, e.g., the  $xy_i$  orbital at site  $\mathbf{i} = (i_x, i_y)$  by  $(-1)^{(i_x + i_y)} xy_i$  (and analogously for  $x^2 - y^2$  and  $3z^2 - r^2$ ) leads to a translationally invariant Hamiltonian with a one-iron unit cell. For comparison with ARPES experiments, however, this gauge transformation has to be undone, which implies that spectral weight at  $\tilde{\mathbf{k}}$  with orbital character  $xy$ ,  $x^2 - y^2$  or  $3z^2 - r^2$  is plotted at  $\mathbf{k} = \tilde{\mathbf{k}} + (\pi, \pi)$ .<sup>18,33</sup>

In order to study a nematic phase, the four-fold lattice symmetry is explicitly broken by introducing a phenomenological Heisenberg interaction, which couples electrons in all orbitals,

$$H_{\text{Heis}} = \pm J_{\text{anis}} \sum_{\langle \mathbf{i}, \mathbf{j} \rangle} \mathbf{S}_{\mathbf{i}\mu} \cdot \mathbf{S}_{\mathbf{j}\nu}, \quad (7)$$

where  $\mu, \nu$  denote orbitals and  $\langle \mathbf{i}, \mathbf{j} \rangle$  nearest-neighbor (NN) bonds. For  $J_{\text{anis}} > 0$ , the coupling is AFM (FM) along the  $x$  ( $y$ ) direction. The electron-spin operators are given by  $\mathbf{S}_{\mathbf{i}\nu} = \frac{1}{2} \sum_{ss'} d_{\mathbf{i}\nu s}^\dagger \boldsymbol{\sigma}_{ss'} d_{\mathbf{i}\nu s'}$ , where  $\boldsymbol{\sigma} = (\sigma^x, \sigma^y, \sigma^z)$  is the vector of Pauli matrices. These interactions act only within the small cluster that is solved exactly. We are here not going to investigate the origin of such a breaking of rotational symmetry, which has been shown to occur in several models,<sup>11,12,14,15</sup> but we will study its impact on the system. We find that when the system is close to the spin-density wave, very small values of  $J_{\text{anis}}$  trigger highly anisotropic band distortions, suggesting that short-range correlations, as observed in a spin-fermion model,<sup>19</sup> indeed favor such a symmetry breaking.

When onsite interactions<sup>34,35</sup> are taken into account, the same values of intra-orbital Coulomb repulsion  $U$ , inter-orbital repulsion  $U'$ , Hund's rule coupling  $J$  and pair hopping  $J' = J$  were used for all orbitals, along with the standard relation  $U' = U - 2J$ , giving

$$H_{\text{int}} = U \sum_{\mathbf{i}, \alpha} n_{\mathbf{i}, \alpha, \uparrow} n_{\mathbf{i}, \alpha, \downarrow} + (U' - J/2) \sum_{\mathbf{i}, \alpha < \beta} n_{\mathbf{i}, \alpha} n_{\mathbf{i}, \beta} \\ - 2J \sum_{\mathbf{i}, \alpha < \beta} \mathbf{S}_{\mathbf{i}, \alpha} \cdot \mathbf{S}_{\mathbf{i}, \beta} \\ + J \sum_{\mathbf{i}, \alpha < \beta} (d_{\mathbf{i}, \alpha, \uparrow}^\dagger d_{\mathbf{i}, \alpha, \downarrow}^\dagger d_{\mathbf{i}, \beta, \downarrow} d_{\mathbf{i}, \beta, \uparrow} + h.c.), \quad (8)$$

where  $\alpha, \beta$  denote the orbital and  $\mathbf{S}_{\mathbf{i}, \alpha}$  ( $n_{\mathbf{i}, \alpha}$ ) is the spin (electronic density) in orbital  $\alpha$  at site  $\mathbf{i}$ . While the parameters relating to the  $xy$  and  $x^2 - y^2$  orbitals can in principle be slightly different from each other and the

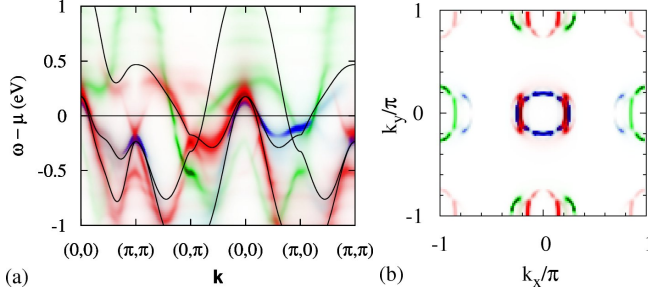


FIG. 2. (Color online) (a) Spectral density  $A(\mathbf{k}, \omega)$  and (b) Fermi surface of the three-orbital model (four-site cluster) with parameters as given for Fig. 1(c) and an explicit symmetry-breaking  $J_{\text{anis}} = 0.5$  eV, see Eq. (7), but without Coulomb repulsion and Hund's rule coupling. Shadings are for “real” momentum, lines indicate the non-interacting model in pseudo-crystal momentum  $\tilde{\mathbf{k}}$ .

$xz/yz$  doublet, symmetric interactions were chosen for simplicity.

### III. RESULTS

#### A. Band anisotropy in the three- and four-orbital models

In order to study the effects of phenomenological short range magnetic correlations, the Hamiltonian given by Eqs. (1) and (7), was initially treated with the VCA on a four-site cluster, with AFM interactions along  $x$  and FM ones along  $y$  but without onsite Coulomb and Hund interactions. A fictitious chemical potential was optimized as a variational parameter, but did not have a large impact on the results. No tendencies towards long-range order were found, which agrees with expectations: Since the AFM Heisenberg interaction only acts within the cluster, it favors a total cluster spin of  $S_{\text{tot}} = 0$ . In the large system, consisting of many noninteracting clusters, there is no magnetic order. Rather large  $J_{\text{anis}} \gtrsim 0.3$  eV has to be chosen to induce appreciable signatures of the anisotropy, which is a very large energy scale compared to the other parameters of the Hamiltonian. The reason is that the non-interacting model with four electrons per site does not contain any net unpaired spins that can directly be coupled by a Heisenberg interaction; the interaction first needs to be strong enough to induce a local spin.

The spectral density for  $J_{\text{anis}} = 0.5$  eV is shown in Fig. 2(a). Apart from the fact that the Heisenberg interactions make the spectrum more incoherent, the bands are most strongly modified near  $X = (\pi, 0)$ , which corresponds to the ordering vector that would be favored by the NN AFM interaction along  $x$ . One clearly sees that the  $yz$  states around  $X$  are moved to higher energies, while the  $xz$  states at  $Y = (0, \pi)$  are shifted to slightly lower energies in agreement with experiments. The energy shifts are momentum dependent: While the

differences between  $X$  and  $Y$  are large, changes around  $\Gamma = (0, 0)$  are far less pronounced. The corresponding orbital-resolved FS can be seen in Fig. 2(b). Like the spectral density, it shows some features that are similar to those resulting from band folding in a  $(\pi, 0)$  SDW; for example, the  $xz$  electron pocket at  $Y$  has a “mirror pocket” at  $M = (\pi, \pi) = Y + (\pi, 0)$ . However, the FS is still qualitatively different from the FS found in the long-range ordered SDW, where folding leads to additional features and largely suppresses the  $yz$  weight,<sup>36</sup> which dominates the hole pockets here. Such differences related to long-range order are consistent with ARPES experiments in NaFeAs,<sup>8</sup> see also the discussion in Sec. III B.

The same behavior as in the three-orbital model is seen for the four-orbital case, see Fig. 3, where  $A(\mathbf{k}, \omega)$  is shown for increasing  $J_{\text{anis}} = 0.2, 0.3, 0.4$  eV. In the last case, the splitting between the states at  $X$  and  $Y$  is  $\approx 150$  meV. Taking into account that the overall band width has to be renormalized by a factor of 2-3, this is consistent with the order of magnitude of the 60 meV splitting reported for  $\text{Ba}(\text{Fe}_{1-x}\text{Co}_x)_2\text{As}_2$ .<sup>7</sup> This can be compared to an explicit orbital splitting, similar to the mechanism proposed in Ref. 18. The splitting can be written as  $\Delta = (n_{yz} - n_{xz})/2$ , where  $n_{xz}$  ( $n_{yz}$ ) is the density in the  $xz$  ( $yz$ ) orbital, and was set to  $\Delta = 0.15$  eV, which approximately reproduces the energy difference between the  $X$  and  $Y$  points indicated by the dashed lines in Fig. 3(c). A momentum-independent splitting large enough to reproduce the energy differences between the  $X$  and  $Y$  points substantially distorts the features near the  $\Gamma$  point as well. While the unoccupied states above the chemical potential at  $\Gamma$  are not easily accessible in ARPES, available data on the bands defining the hole pockets appear more consistent with the slighter changes caused by momentum-dependent shifts of the nematic scenario, especially for cases with a large splitting between the features near  $X/Y$ , where the bands near  $\Gamma$  would be very strongly distorted by a rigid shift.<sup>7-10</sup>

Total orbital densities do not turn out to be a reliable way to characterize the impact of the nematic order on states near the Fermi energy. Densities in the  $xz$  and  $yz$  orbitals differ only slightly in the four-orbital model with  $n_{xz} - n_{yz} \approx 0.02$  for  $J_{\text{anis}} = 0.4$  eV. This value is not strongly affected by 4% hole or electron doping, in contrast to a proposed sign change for hole doping<sup>14</sup> and it is broadly consistent with the small orbital polarizations found in mean-field analyses for the SDW state.<sup>23,36</sup> In the three-orbital model, the orbital polarization is even *opposite* with  $n_{xz} - n_{yz} \approx -0.1$ , because spectral weight with  $yz$  character is transferred below the Fermi level [see the density of states shown in Fig. 4(a)], and in contrast to the four-orbital model [see Fig. 4(b)], this weight is not balanced by  $xz$  states further away from  $\mu$ . Nevertheless, the band reconstruction near the Fermi level and the band anisotropy are very similar in the two models. AFM correlations along  $x$  always bring the  $yz$  states around  $X$  closer to the Fermi level, even when the total orbital densities satisfy  $n_{yz} > n_{xz}$ , in contrast to

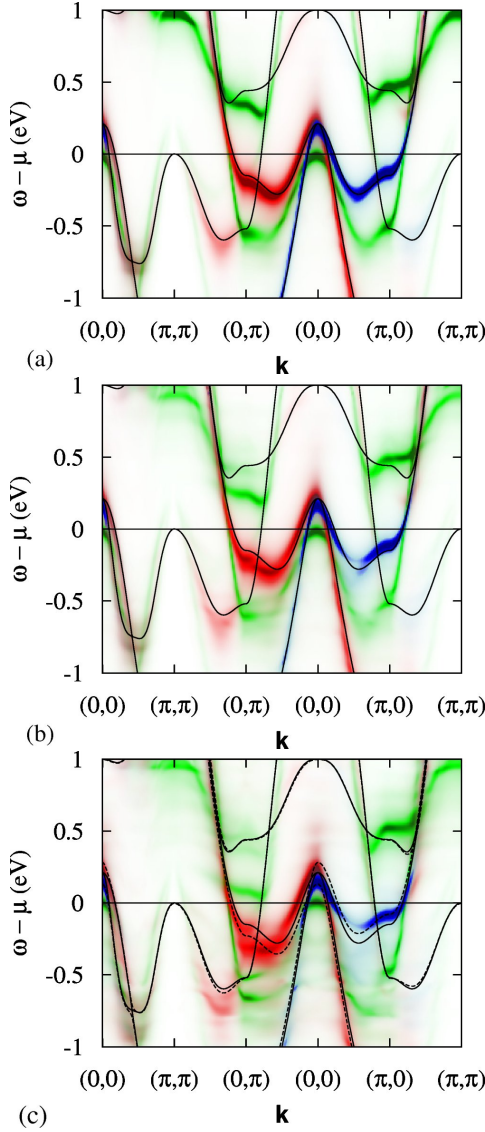


FIG. 3. (Color online) Spectral density  $A(\mathbf{k}, \omega)$  of the four-orbital model (three-site cluster), see Fig. 1(d), and an increasing explicit symmetry-breaking term Eq. (7) of (a)  $J_{\text{anis}} = 0.2$  eV, (b)  $J_{\text{anis}} = 0.3$  eV, and (c)  $J_{\text{anis}} = 0.4$  eV. Coulomb repulsion and Hund’s rule coupling are not included. Shadings are for “real” momentum, solid lines indicate the non-interacting model in pseudo-crystal momentum  $\mathbf{k}$ . In (c), dashed lines are for a non-interacting model with an energy difference  $\Delta = 0.15$  eV between the  $xz$  and  $yz$  orbitals, which was fitted to approximately reproduce the difference between the  $X$  and  $Y$  points.

a naive expectation that the  $yz$  bands should be lowered in energy in this case. When onsite interactions bring the three-orbital model closer to the SDW transition (see Sec. IIIB below), the orbital densities become almost equal with  $n_{xz} - n_{yz} \approx -0.012$  for  $U = 1$  eV. Total orbital densities can determine magnetic properties via the Goodenough-Kanamori rules in Mott insulators, which do not have a FS. On the other hand, since the

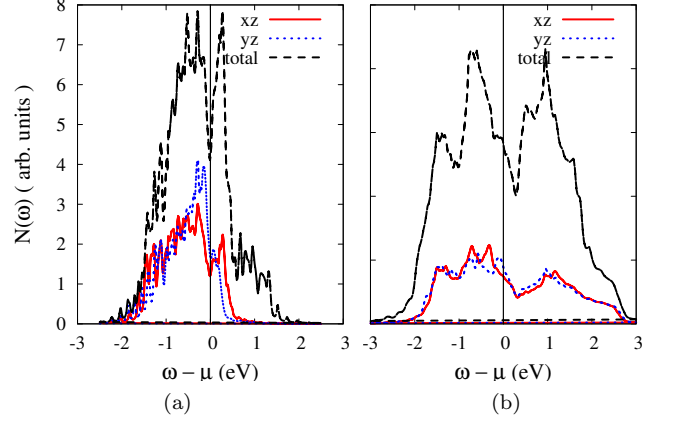


FIG. 4. (Color online) Density of states for (a) the three-orbital model with  $J_{\text{anis}} = 0.5$  eV and (b) the four-orbital model and  $J_{\text{anis}} = 0.4$  eV.  $U = J_{\text{Hund}} = 0$  in both cases.

pnictides are more metallic with strongly hybridized orbitals, a more consistent and clearer picture can here be obtained if one concentrates on spectral weight near the Fermi level as will be discussed below.

## B. Impact of onsite Coulomb interaction

In this subsection the impact of onsite interactions will be investigated. The full Eq. (8) including spin-flip and pair-hopping terms can easily be included in the VCA. Interaction strengths were chosen below the critical values for the onset of long-range order because we want to focus on short-range correlations here. As can be seen in Fig. 5 for the two models considered here, lower values of  $J_{\text{anis}} \approx 0.2$  is now sufficient to induce substantial asymmetries, in contrast to the larger  $J_{\text{anis}} \approx 0.4$  to  $0.5$  eV needed for the noninteracting models. Onsite interactions favor local magnetic moments, even in the absence of long-range order, that can then be coupled even by weaker  $J_{\text{anis}}$ .

Finally, we study the three-orbital model very close to the SDW transition by setting  $U = 1.02$  eV. In a mean-field treatment as used in Ref. 23, one finds an SDW with long-range magnetic order, but the optimal VCA solution does not yet show long-range order due to the presence of quantum fluctuations. However, the system is so close to a magnetically ordered state that very small  $J_{\text{anis}} \approx 0.015$  eV = 15 meV already introduces strong short-range order and corresponding band anisotropies. Several occupied low-energy bands [e.g. between  $\Gamma = (0,0)$  and  $Y = (0,\pi)$  as well as around  $M = (\pi,\pi)$ ] in the spectral density, which is shown in Fig. 5(c), have energies reduced by a factor of  $\approx 2$ , consistent with the renormalization factor  $\approx 2 - 3$  needed to reconcile density-functional bands with ARPES. Bands above the Fermi level do not have reduced widths. This asymmetric impact of correlations is in agreement with



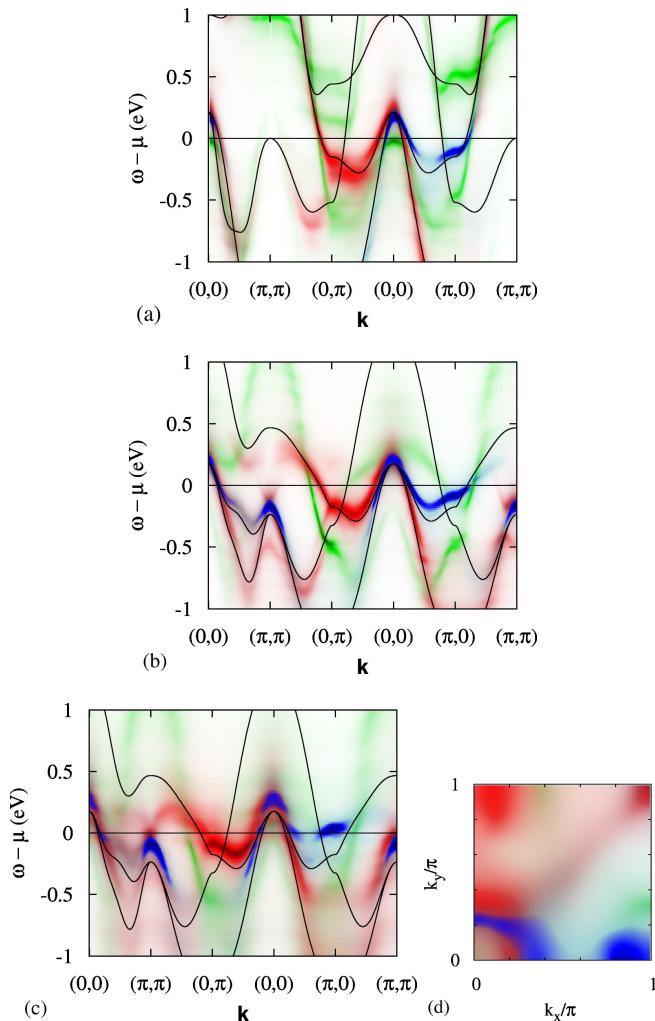


FIG. 5. (Color online) Spectral density with anisotropic short-range magnetic order and onsite interactions. (a) For the four-orbital model and  $U = 0.3$  eV,  $J_{\text{Hund}} = 0.075$  eV and  $J_{\text{anis}} = 0.2$  eV. (b) For the three-orbital model with  $U = 0.6$  eV ( $J_{\text{Hund}} = 0.15$  eV) and  $J_{\text{anis}} = 0.2$  eV and (c)  $U = 1.02$  eV ( $J_{\text{Hund}} = 0.255$  eV) and  $J_{\text{anis}} = 0.015$  eV. For these last values of  $U$  and  $J_{\text{Hund}}$ , the three-orbital model is very close to the SDW. (d) FS corresponding to the parameters in (c), it captures spectral weight within 1 meV of the Fermi level; broadening of the spectral weight is consistent with (c). Onsite interactions are lower for the four-orbital model, because it is at half filling and Hund’s rule thus, moves it closer to a Mott transition, while it partly compensates  $U$  away from half filling, as in the three-orbital model. Shadings are for “real” momentum; lines indicate the non-interacting model in pseudo-crystal momentum  $\tilde{\mathbf{k}}$ .

dynamical mean-field studies.<sup>37</sup> In addition to the renormalization,  $J_{\text{anis}} = 15$  meV induces an energy splitting of  $\approx 70$  meV between the  $X$  and  $Y$  points. In fact, the band at  $X$  has moved slightly *above the chemical potential*, as expected for the SDW phase. The fact, that this happens even in the absence of long-range order, is in excellent agreement with recent ARPES data for NaFeAs,

where it was likewise found that the overall band positions at  $X$  and  $Y$  nearly reach their “SDW values” above the Néel temperature.<sup>8</sup>

Nevertheless, the corresponding FS, see Fig. 5(d), clearly shows important differences to that of the SDW state: As the  $yz$  states cross the chemical potential here with a rather low Fermi velocity (leading to an elongation of the hole pocket at  $\Gamma$  along the  $x$ -direction), they contribute substantial weight to the FS. In fact, both of the strong features along the  $\Gamma$ - $X$  line are of  $yz$  character. In the SDW phase, in contrast, the  $yz$  orbital dominates the AFM order parameter and is thus mostly gapped out.<sup>36</sup> Related effects have likewise been observed in ARPES, where these  $yz$  bands open gaps at the Néel temperature.<sup>8,38</sup>

#### IV. SUMMARY AND CONCLUSIONS

The variational cluster approach was used to study the spectral density of a nematic phase in three- and four-orbital models for iron-based superconductors. We found that the method is well suited for problems involving short-range correlations without long-range (magnetic) order. The correlations considered in this study were extremely short-range, going only over NN sites, the minimum to break rotational invariance. While this is a somewhat extreme scenario, it has been argued that magnetic correlations that are effective only on a very short range lead to the linear temperature dependence of the magnetic susceptibility at high temperatures.<sup>39</sup> Nuclear quadrupole resonance<sup>40</sup> indicates that there are As ions seeing different electronic surroundings in the “underdoped regime”, which would be in agreement with the present scenario of As ions involved in “magnetic” vs. “non-magnetic” bonds.

When symmetry between the  $x$ - and  $y$  directions is broken by a phenomenological magnetic interaction that is AFM in the  $x$  direction, the bands with  $yz$  character around momentum  $X = (\pi, 0)$  move to higher energies, i.e., closer to the Fermi level. This is in agreement with ARPES on detwinned samples above the magnetic transition temperature, in both the “122” compound  $\text{Ba}(\text{Fe}_{1-x}\text{Co}_x)_2\text{As}_2$ ,<sup>7</sup> and the “111” compound  $\text{NaFeAs}$ .<sup>8,10</sup> The latter is not expected to have surface states<sup>41</sup> that might complicate the analysis of ARPES in 122 compounds.<sup>42</sup> The changes in the band structure due to the nematic order not only depend on the orbital, but also on momentum. Changes around the  $\Gamma = (0, 0)$  point are far less pronounced than differences between  $X$  and  $Y$ , again in agreement with ARPES.<sup>8–10</sup> Total orbital densities and their difference are model dependent and not a reliable predictor of reconstructions of low-energy states. However, the orbital-resolved spectral weight and the bands near the Fermi level are affected in the same way both in a three- and a four-orbital model, with and without onsite interactions indicating that they are more universal and less dependent on details of the

model Hamiltonian. In agreement with previous findings on the orbital polarization of the FS in the SDW phase<sup>36</sup> and on transport properties,<sup>19,43</sup> this suggests that total (orbital) densities are here less important than in Mott insulators, as the metallic character of the pnictides makes states near the Fermi level far more important than those further away.

When onsite interactions are strong enough to bring the system close to the SDW transition, very small anisotropic couplings can deform the bands until their broad features resemble bands in the SDW regime, i.e., bands are renormalized by a factor of  $\approx 2$  and the  $yz$  states at  $X$  move above the chemical potential, as seen in ARPES on NaFeAs just above the Néel temperature.<sup>8</sup>

Nevertheless, the Fermi surface still differs from that of a state with full long-range magnetic order, where the  $yz$  states are mostly gapped out,<sup>36,38</sup> again in agreement with ARPES.<sup>8</sup>

## ACKNOWLEDGMENTS

This research was sponsored by the Deutsche Forschungsgemeinschaft (DFG) under the Emmy-Noether program, the NSF grant DMR-1104386, and the Division of Materials Science and Engineering, Office of Basic Energy Sciences, U.S. DOE. We thank Philip Brydon and Jeroen van den Brink for helpful discussion.

- 
- \* M.Daghofer@ifw-dresden.de
- <sup>1</sup> D. Johnston, *Advances in Physics* **59**, 803 (2010).
  - <sup>2</sup> J. Paglione and R. L. Greene, *Nature Physics* **6**, 645 (2010).
  - <sup>3</sup> L. Boeri, O. V. Dolgov, and A. A. Golubov, *Phys. Rev. Lett.* **101**, 026403 (2008).
  - <sup>4</sup> C. de la Cruz, Q. Huang, J. W. Lynn, J. Li, W. R. II, J. L. Zarestky, H. A. Mook, G. F. Chen, J. L. Luo, N. L. Wang, and P. Dai, *Nature* **453**, 899 (2008).
  - <sup>5</sup> J.-H. Chu, J. G. Analytis, K. D. Greve, P. L. McMahon, Z. Islam, Y. Yamamoto, and I. R. Fisher, *Science* **329**, 824 (2010).
  - <sup>6</sup> A. Dusza, A. Lucarelli, F. Pfner, J. Chu, I. Fisher, and L. Degiorgi, *EPL* **93**, 37002 (2011).
  - <sup>7</sup> M. Yi, D. H. Lu, J.-H. Chu, J. G. Analytis, A. P. Sorini, A. F. Kemper, S.-K. Mo, R. G. Moore, M. Hashimoto, W. S. Lee, Z. Hussain, T. P. Devereaux, I. R. Fisher, and Z.-X. Shen, *PNAS* **108**, 6878 (2011).
  - <sup>8</sup> M. Yi, D. H. Lu, R. G. Moore, K. Kihou, C.-H. Lee, A. Iyo, H. Eisaki, T. Yoshida, A. Fujimori, and Z.-X. Shen, *arXiv:1111.6134*.
  - <sup>9</sup> C. He, Y. Zhang, B. P. Xie, X. F. Wang, L. X. Yang, B. Zhou, F. Chen, M. Arita, K. Shimada, H. Namatame, M. Taniguchi, X. H. Chen, J. P. Hu, and D. L. Feng, *Phys. Rev. Lett.* **105**, 117002 (2010).
  - <sup>10</sup> Y. Zhang, C. He, Z. R. Ye, J. Jiang, F. Chen, M. Xu, Q. Q. Ge, B. P. Xie, J. Wei, M. Aeschlimann, X. Y. Cui, M. Shi, J. P. Hu, and D. L. Feng, *Phys. Rev. B* **85**, 085121 (2012).
  - <sup>11</sup> C. Fang, H. Yao, W.-F. Tsai, J. Hu, and S. A. Kivelson, *Phys. Rev. B* **77**, 224509 (2008).
  - <sup>12</sup> C. Xu, M. Müller, and S. Sachdev, *Phys. Rev. B* **78**, 020501 (2008).
  - <sup>13</sup> F. Krüger, S. Kumar, J. Zaanen, and J. van den Brink, *Phys. Rev. B* **79**, 054504 (2009).
  - <sup>14</sup> R. M. Fernandes, A. V. Chubukov, J. Knolle, I. Eremin, and J. Schmalian, *Phys. Rev. B* **85**, 024534 (2012).
  - <sup>15</sup> A. Cano, M. Civelli, I. Eremin, and I. Paul, *Phys. Rev. B* **82**, 020408 (2010).
  - <sup>16</sup> P. M. R. Brydon and C. Timm, *Phys. Rev. B* **79**, 180504 (2009).
  - <sup>17</sup> I. Paul, *Phys. Rev. Lett.* **107**, 047004 (2011).
  - <sup>18</sup> W. Lv and P. Phillips, *Phys. Rev. B* **84**, 174512 (2011).
  - <sup>19</sup> S. Liang, G. Alvarez, C. Şen, A. Moreo, and E. Dagotto, *arXiv:1111.6994*.
  - <sup>20</sup> R. M. Fernandes, E. Abrahams, and J. Schmalian, *Phys. Rev. Lett.* **107**, 217002 (2011).
  - <sup>21</sup> C. Gros and R. Valentí, *Phys. Rev. B* **48**, 418 (1993).
  - <sup>22</sup> D. Sénéchal, D. Perez, and M. Pioro-Ladrière, *Phys. Rev. Lett.* **84**, 522 (2000).
  - <sup>23</sup> M. Daghofer, A. Nicholson, A. Moreo, and E. R. Dagotto, *Phys. Rev. B* **81**, 014511 (2010).
  - <sup>24</sup> R. Yu and Q. Si, *Phys. Rev. B* **84**, 235115 (2011).
  - <sup>25</sup> S. Graser, T. A. Maier, P. J. Hirschfeld, and D. J. Scalapino, *New J. Phys.* **11**, 025016 (2009).
  - <sup>26</sup> M. Potthoff, M. Aichhorn, and C. Dahnken, *Phys. Rev. Lett.* **91**, 206402 (2003).
  - <sup>27</sup> C. Dahnken, M. Aichhorn, W. Hanke, E. Arrigoni, and M. Potthoff, *Phys. Rev. B* **70**, 245110 (2004).
  - <sup>28</sup> M. Daghofer, A. Moreo, J. A. Riera, E. Arrigoni, D. J. Scalapino, and E. R. Dagotto, *Phys. Rev. Lett.* **101**, 237004 (2008).
  - <sup>29</sup> R. Yu, K. T. Trinh, A. Moreo, M. Daghofer, J. A. Riera, S. Haas, and E. R. Dagotto, *Phys. Rev. B* **79**, 104510 (2009).
  - <sup>30</sup> P. Brydon, M. Daghofer, and C. Timm, *J. Phys.: Condens. Matter* **23**, 246001 (2011).
  - <sup>31</sup> P. A. Lee and X.-G. Wen, *Phys. Rev. B* **78**, 144517 (2008).
  - <sup>32</sup> H. Eschrig and K. Koepernik, *Phys. Rev. B* **80**, 104503 (2009).
  - <sup>33</sup> S.-H. Lee, G. Xu, W. Ku, J. Wen, C. Lee, N. Katayama, Z. Xu, S. Ji, Z. Lin, G. Gu, H.-B. Yang, P. Johnson, Z.-H. Pan, T. Valla, M. Fujita, T. Sato, S. Chang, K. Yamada, and J. Tranquada, *Phys. Rev. B* **81**, 220502 (2010).
  - <sup>34</sup> C. Castellani, C. R. Natoli, and J. Ranninger, *Phys. Rev. B* **18**, 4945 (1978).
  - <sup>35</sup> A. M. Oleś, *Phys. Rev. B* **28**, 327 (1983).
  - <sup>36</sup> M. Daghofer, Q.-L. Luo, R. Yu, D. X. Yao, A. Moreo, and E. R. Dagotto, *Phys. Rev. B* **81**, 180514(R) (2010).
  - <sup>37</sup> M. Aichhorn, L. Pourovskii, V. Vildosola, M. Ferrero, O. Parcollet, T. Miyake, A. Georges, and S. Biermann, *Phys. Rev. B* **80**, 085101 (2009).
  - <sup>38</sup> T. Shimojima, K. Ishizaka, Y. Ishida, N. Katayama, K. Ohgushi, T. Kiss, M. Okawa, T. Togashi, X. Y. Wang, C. T. Chen, S. Watanabe, R. Kadota, T. Oguchi, A. Chainani, and S. Shin, *Phys. Rev. Lett.* **104**, 057002 (2010).
  - <sup>39</sup> R. Klingeler, N. Leps, I. Hellmann, A. Popa, U. Stockert, C. Hess, V. Kataev, H.-J. Grafe, F. Hammerath, G. Lang, S. Wurmehl, G. Behr, L. Harnagea, S. Singh,

- and B. Büchner, Phys. Rev. B **81**, 024506 (2010).
- <sup>40</sup> G. Lang, H.-J. Grafe, D. Paar, F. Hammerath, K. Manthey, G. Behr, J. Werner, and B. Büchner, Phys. Rev. Lett. **104**, 097001 (2010).
- <sup>41</sup> A. Lankau, K. Koepnik, S. Borisenko, V. Zabolotnyy, B. Büchner, J. van den Brink, and H. Eschrig, Phys. Rev. B **82**, 184518 (2010).
- <sup>42</sup> E. van Heumen, J. Vuorinen, K. Koepnik, F. Massee, Y. Huang, M. Shi, J. Klei, J. Goedkoop, M. Lindroos, J. van den Brink, and M. S. Golden, Phys. Rev. Lett. **106**, 027002 (2011).
- <sup>43</sup> X. Zhang and E. Dagotto, Phys. Rev. B **84**, 132505 (2011).